Microchimica Acta (2021) 188: 39
https://doi.org/10.1007/s00604-020-04698-6

ORIGINAL PAPER

Simultaneous electrochemical determination of *nuc* and *mecA* genes for identification of methicillin-resistant *Staphylococcus aureus* using N-doped porous carbon and DNA-modified MOF

Ge Dai[1] · Zhi Li[1] · Feifei Luo[1] · Yuqi Lu[1] · Zhaohui Chu[1] · Jingwen Zhang[1] · Fan Zhang[1] · Qingjiang Wang[1] · Pingang He[1]

Received: 1 August 2020 / Accepted: 31 December 2020 / Published online: 12 January 2021

Abstract

The detection of *Staphylococcus aureus* specific gene in combination with the *mecA* gene is vitally important for accurate identification of methicillin-resistant *Staphylococcus aureus* (MRSA). A homogeneous electrochemical DNA sensor was fabricated for simultaneous detection of *mecA* and *nuc* gene in MRSA. Metal-organic framework (type UiO-66-NH_2) was applied as nanocarrier. Two electroactive dyes, methylene blue (MB) and epirubicin (EP), were encapsulated in UiO-66-NH_2, respectively, and were locked by the hybrid double-stranded DNA. Based on the target-response electroactive dye release strategy, once target DNA exists, it completely hybridizes with displacement DNA (D_{EP} and D_{MB}). So D_{EP} and D_{MB} is displaced from the MOF surface, causing the release of electroactive dyes. Co-Zn bimetallic zeolitic imidazolate framework-derived N-doped porous carbon serves for electrode modification to improve electrocatalytic performance and sensitivity. The differential pulse voltammetry peak currents of MB and EP were accurately detected at − 0.14 V and − 0.53 V versus the Ag/AgCl reference electrode, respectively. Under the optimal conditions, the detection limits of *mecA* gene and *nuc* gene were 3.7 fM and 1.6 fM, respectively. Combining the effective application of MOFs and the homogeneous detection strategy, the sensor exhibited satisfactory performance for MRSA identification in real samples. The recovery was 92.6–103%, and the relative standard deviation was less than 5%. Besides, MRSA and SA can also be distinguished. This sensor has great potential in practical applications.

Keywords Electrochemical DNA sensor · Modified electrode · Differential pulse voltammetry · UiO-66 · Co-Zn bimetallic ZIF · Foodborne bacteria

Introduction

Staphylococcus aureus (SA) is responsible for a large number of foodborne infections, and the antibiotic-resistant strains of SA are becoming a severe threat to human health worldwide [1]. Methicillin-resistant *Staphylococcus aureus* (MRSA) is one of the most common pathogens of nosocomial and community infection, leading to increased rate of morbidity and mortality [2]. Considering the urge need of infection control and treatment, rapid and accurate detection of MRSA is extremely important. Various methods have been developed for MRSA detection, such as microarray, next-generation sequencing (NGS), enzyme-linked immune-absorbent assay (ELISA), and surface plasmon resonance (SPR) [3–6]. Although these methods offer specificity and accuracy, they often suffer from one or more disadvantages such as high cost, time-consuming operations, and fussy sample treatment, which hamper their practical application.

Electrochemical DNA sensors have shown great superiority in respect of low cost, time saving, and simple operation [7]. Until now, electrochemical DNA sensors have been effectively applied in bacteria detection. Most electrochemical DNA sensors for MRSA detection only focus on the *mecA*

✉ Fan Zhang
fzhang@chem.ecnu.edu.cn

✉ Qingjiang Wang
qjwang@chem.ecnu.edu.cn

[1] School of Chemistry and Molecular Engineering, East China Normal University, 500 Dongchuan Road, Shanghai 200241, People's Republic of China

gene [8]. Although the test results are satisfactory, it is necessary to identify methicillin resistance together with SA for the aim of therapy and epidemiology [9]. Identification of MRSA depends on the combination of SA specific genes and *mecA* gene detection [10]. The *nuc* gene encodes thermostable *nuc*-leases that are specific to SA [11]. The *mecA* gene codes for penicillin-binding protein (PBP2a or PBP2′) that gives rise to methicillin resistance [12]. The homogeneous electrochemical strategy is a great way to achieve multiple target detection, label-free procedure, and enzyme-free signal amplification [13]. So it is significant to design a homogeneous electrochemical DNA sensor for simultaneous detection of *nuc* and *mecA* gene in MRSA.

The application of functional materials in electrochemical sensors is an effective strategy to enhance performance [14, 15]. As the new class of porous crystalline nanomaterials, metal-organic frameworks (MOFs) have excellent properties such as incredibly high surface area and porosity and favorable biocompatibility [16]. Recently, MOFs have been applied and exhibited considerable advantages in electrochemical sensors [17, 18]. It should be admitted that the suboptimal conductivity of MOFs has limited its further electrochemical application. Ingeniously, MOFs have been discovered as stimuli-responsive porous materials for substrate encapsulation and release [19]. By modifying different molecule gates, the "open" state of pores can be caused by special stimuli. So the encapsulated substrates can be released [20]. Different DNA molecule gates, such as dsDNA, guanosine-rich sequences, and cytosine-rich strands, can be used as capping units [21]. It is worth noting that the stimuli-responsive DNA-gated MOF has not been applied in bacteria detection. Besides, the stimuli-responsive DNA-gated MOF is often applied in the electrochemical biosensing alone, and no other signal-amplifying materials are used, which affect the performance of biosensor. Therefore, it is necessary to combine the stimuli-responsive DNA-gated MOF with suitable signal-amplifying material, which benefits the fabrication of the high sensitivity biosensor.

Attributing to the numerous merits such as rich nitrogen atoms and highly microporous structure [22], zeolitic imidazolate frameworks (ZIFs) have been delicately designed as satisfactory precursors and templates to synthesize N-doped porous carbons (NPC). The ZIF-8-derived NPC affords the large surface area, but it cannot provide good graphitized carbon. The ZIF-67-derived NPC has been demonstrated to offer highly graphitized carbon, whereas the obtaining of large surface area is tough. The Co-Zn bimetallic ZIF (BMZIF)-derived NPC combines both advantages of carbons independently from ZIF-8 and ZIF-67 [23], including the large surface area and high graphitization degree, which benefits the electrical conductivity and electrocatalysis. To our knowledge, the research on BMZIF-derived NPCs for electrochemical DNA sensors is rare.

Thus, the UiO-66-NH_2 and BMZIF-derived NPC-based homogeneous electrochemical DNA sensor was fabricated for simultaneous detection of *nuc* gene and *mecA* gene in MRSA. The UiO-66-NH_2 was loaded with methylene blue (MB) and epirubicin (EP) respectively and was capped by double-stranded DNA (dsDNA). BMZIF-derived NPCs were applied to modify the electrode for enhancement of the sensitivity. The MB and EP would be released from the DNA-gated UiO-66-NH_2 upon the target gene existed. Under the optimal conditions, the *nuc* gene and *mecA* gene were quantitatively detected through the DPV current changes of EP and MB. This sensor is capable to identify MRSA and distinguish MRSA and SA, which is promising for further application in medicine and biology.

Materials and methods

Reagents and apparatus

The reagents and apparatus are given in Section S1 of Electronic Supporting Material.

Synthesis of Co-Zn bimetallic ZIF-derived N-doped porous carbon

Co-Zn bimetallic ZIF was prepared as follows. First, 0.80 g of $Zn(NO_3)_2.6H_2O$ and 0.038 g of $Co(NO_3)_2.6H_2O$ were dissolved in 40 mL of methanol by sonication. In the reactants, the Zn/Co molar ratio was 20. Then 40 mL of methanol containing 1.80 g of 2-methylimidazole was added into the above solution. The mixture was stirred vigorously for 24 h at room temperature. The product was collected by centrifugation and washed successively with methanol. Finally, the Co-Zn bimetallic ZIF was dried at 80 °C under vacuum for 12 h. The Co-Zn bimetallic ZIF was heated to 900 °C at a heating rate of 5 °C min^{-1}. Then the sample was carbonized at 900 °C for 2 h and cooled to room temperature naturally. The whole process was under a nitrogen gas flow. To synthesize the NPC containing graphitic frameworks, the deposited Zn and Co nanoparticles were removed with HF aqueous solution (10 wt%), resulting in a highly porous structure. The product was washed thoroughly with water. Finally, the NPC was vacuum dried at 120 °C overnight.

Synthesis of UiO-66-NH_2

0.03 g of zirconium chloride ($ZrCl_4$) and 0.03 g of 2-aminoterephthalic acid were dissolved in 20 mL of dimethyl formamide (DMF) by sonication. Subsequently, 0.5 g of glacial acetic acid was added as a modulator. The mixture was reacted at 120 °C for 24 h. The product was collected by centrifugation and washed with DMF several times. After that,

the product was soaked in DMF for 12 h to remove the unreacted reagents. Finally, the UiO-66-NH_2 was washed with acetone and dried at 60 °C under vacuum for 12 h.

Synthesis of EP@UiO and MB@UiO

For EP@UiO preparation, 500 μL of C_{EP}, 500 μL of 1-ethyl-3-(3-dimethylaminopropyl) carbodiimide (EDC, 5 mg mL^{-1}), and 500 μL of N-hydroxysulfosuccinimide (NHS, 5 mg mL^{-1}) were mixed and reacted under gentle shaking for 30 min. Then 0.01 g UiO-66-NH_2 were added, and the mixture was reacted overnight under gentle shaking. The carboxylated C_{EP} was assembled on UiO-66-NH_2 through the amidation reaction [24]. The C_{EP}-modified UiO-66-NH_2 was washed with phosphate buffer (PB) three times to remove the unbound C_{EP} and dispersed in 1.5 mL PB. For EP loading, 200 μL of C_{EP}-modified UiO-66-NH_2 was incubated with 40 μL of EP solution (1.2 mM) for 24 h. Subsequently, 160 μL D_{EP} was added, and the mixture was reacted for 1 h to yield the dsDNA-modified UiO-66-NH_2 (EP@UiO). Finally, the EP@UiO were washed with PB several times and dispersed in 500 μL of PB. MB@UiO was synthesized in accordance with the above steps. C_{MB}, MB solution (1.2 mM), and D_{MB} were used in the MB@UiO synthesis.

Fabrication of the modified electrode

The bare GCE was firstly polished with 0.3- and 0.05-μm alumina slurry until mirrorlike. Then the GCE was ultrasonicated in ethanol and water successively and dried under nitrogen. Subsequently, N-doped porous carbon materials were dispersed in ethanol and N-butyl alcohol mixture by ultrasound. Finally, 2 μL of dispersion (1 mg mL^{-1}) was dropped on the GCE surface and dried in infrared drying oven. The modified electrode was denoted as NPC/GCE.

Electrochemical detection

For simultaneous detection of *nuc* gene and *mecA* gene, 40 μL of EP@UiO, 40 μL of MB@UiO, and 80 μL of target DNA containing different concentration of *nuc* gene and *mecA* gene were incubated for 1.0 h. After that, PB was added to the mixture to obtain a test solution with total volume of 500 μL. DPV was performed at the scan rate of 100 mV s^{-1}.The potential ranged from 0.2 to − 0.6 V. The DPV peak potentials of MB and EP were − 0.14 V and − 0.53 V, respectively.

PCR of bacteria DNA and gel electrophoresis

PCR conditions were set up according to our published articles [25]. The detailed process of PCR and gel electrophoresis is given in Section S2 of Electronic Supporting Material.

Real sample pretreatment

The pretreatments of the tap water were as follows. Firstly, in order to decontaminate, tap water was purified by a 22-μM membrane and sterilized. Secondly, different concentrations of MRSA (10^2 - 10^6 CFU mL^{-1}) were inoculated into 1 mL purified tap water, respectively. Then the inoculated tap water was centrifuged at 6000 rpm for 10 min. After that, the DNA of MRSA was extracted and amplified by PCR. The PCR products were detected by DPV, respectively.

Four purified milk samples were sterilized to remove bacterial contaminants. No bacteria were detected in the samples by the standard plate counting method. Then the milk samples were inoculated different concentrations of MRSA. According to the European Union Commission standard for food microbiology (No. 1441/2007), the bacteria concentration of milk and dairy products should not exceed 10^4 CFU mL^{-1}. So the spiked concentrations of the bacteria were 10^3 and 10^4 CFU mL^{-1}. The samples 1 and 2 were inoculated with 10^4 CFU mL^{-1} MRSA and 10^4 CFU mL^{-1} SA, respectively. While the sample 3 was inoculated with 10^3 CFU mL^{-1} MRSA and 10^4 CFU mL^{-1} SA, the sample 4 was inoculated with 10^4 CFU mL^{-1} MRSA and 10^4 CFU mL^{-1} SA. The samples were centrifuged at 6000 rpm for 10 min. Then the bacteria DNA was extracted and amplified by PCR. The PCR products were denatured by boiling water for 10 min and cooled by ice for 2 min. Each PCR product was detected by DPV, respectively.

Results and discussion

Mechanism of the electrochemical DNA sensor

The principle of the homogeneous electrochemical DNA sensor is described in Scheme 1. As shown in Scheme 1a, the GCE was modified by Co-Zn bimetallic zeolitic imidazolate framework (BMZIF)-derived N-doped porous carbon to improve the electrocatalytic performance and sensitivity. The target-response electroactive dye release strategy was depicted in Scheme 1b. First, the carboxyl-modified ssDNA (C_{EP}) was conjugated to the UiO-66-NH_2 nanocarrier through the amidation reaction. Then the electroactive dyes (EP) were loaded in the pores of UiO-66-NH_2. After that, D_{EP}, which is partially complementary to C_{EP} and completely complementary to target DNA, was hybridized with C_{EP}. The electroactive dye-encapsulated UiO-66-NH_2 was capped by hybrid dsDNA. So the stimuli-responsive DNA-gated MOFs (EP@UiO) were formed. MB@UiO were formed similarly. In the absence of target DNA, the dsDNA capping kept the EP and MB trapped in MOFs. So the DPV signal was extremely small (curve a). Once both target DNA existed, the *mecA* gene

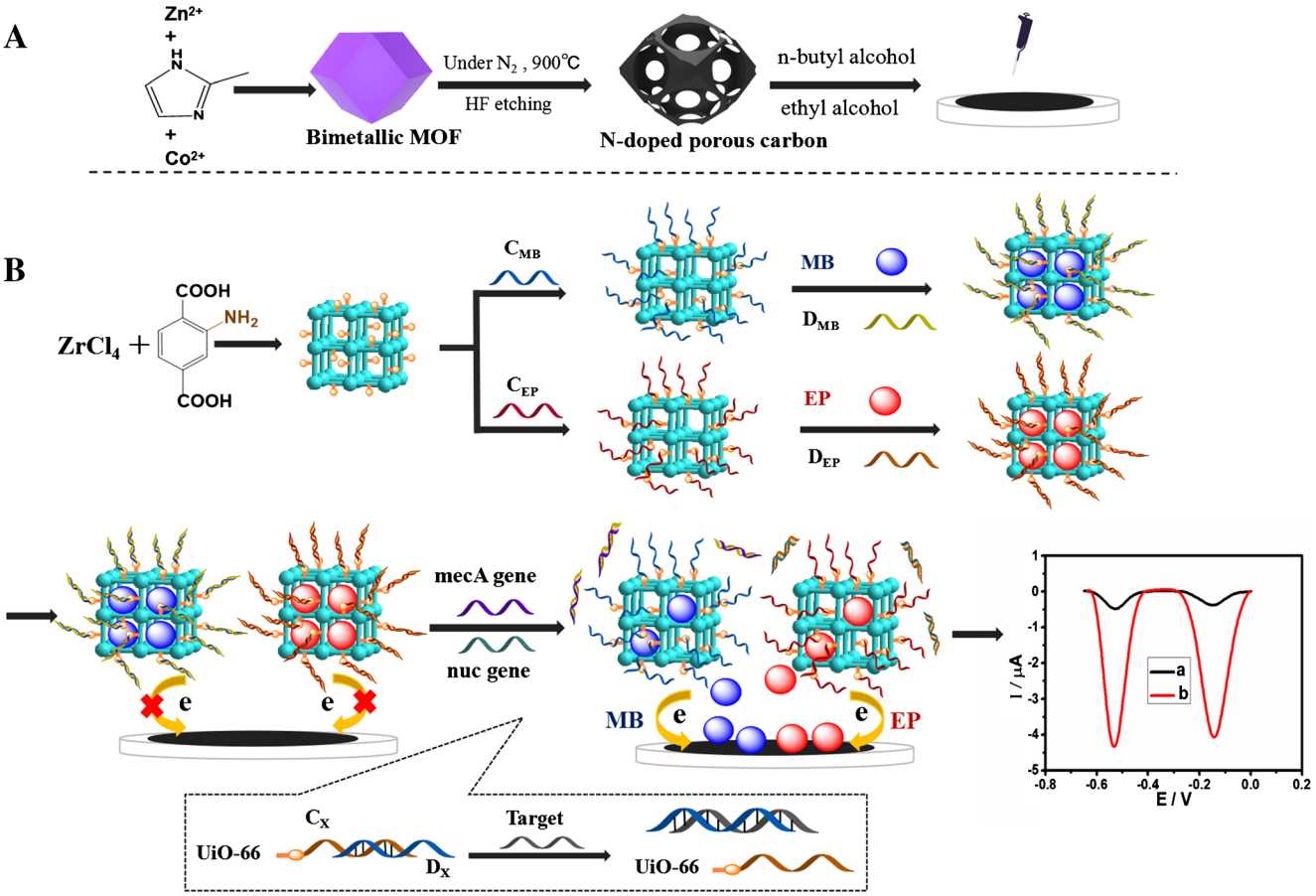

Scheme 1 Schematic illustration of the electrochemical DNA sensor. (**a**) Synthesis of the BMZIF-derived NPC and the electrode modification process. (**b**) Synthesis of the DNA-gated UiO-66 and the schematic principle of simultaneous detection of *mecA* and *nuc* gene. *MB* methylene blue, *EP* epirubicin, C_X (C_{EP}, C_{MB}) capture DNA, D_X (D_{EP}, D_{MB}) displacement DNA

would completely hybridize with D_{MB}, while the *nuc* gene would hybridize with D_{EP}. Therefore, D_{MB} and D_{EP} were displaced from the MOF surface. C_{MB} and C_{EP} were remained on the surface. In this state, EP and MB were synchronously released into the sensing solution. As such, two strong electrical signals were detected by DPV (curve b). Therefore, *nuc* gene and *mecA* gene were detected simultaneously by the changes of the two DPV currents.

Characterization of the materials

SEM was carried out to characterize the morphology of BMZIF and NPC materials. As can be seen from Fig. 1a, the Co-Zn BMZIF has the unique rhombic dodecahedron morphology with an average size of 50 nm. After carbonization, the NPC nanomaterials are well uniform. The original size of the BMZIF precursor is kept. Besides, the original polyhedral shape retains roughly. These results illustrate BMZIF nanocrystalline, and its derived NPC nanomaterials are successfully synthesized. The crystalline structures of BMZIF, ZIF-8, ZIF-67, and NPC were characterized by XRD technique (Fig. S1). The elemental mappings of NPC were shown in Fig. S2.

The morphology of the UiO-66-NH_2 was characterized by SEM (Fig. S3). XRD technique was used to analyze the formation of dsDNA-capped MOFs (EP@UiO and MB@UiO). As shown in Fig. 2a, the XRD patterns of the EP@UiO and MB@UiO exhibit characteristic diffraction peak that are consistent with the diffraction peaks of UiO-66-NH_2. The results suggest that the structure and high crystallinity of UiO-66-NH_2 still remained after the capsulation of electroactive dyes (EP and MB). FT-IR spectra were conducted to verify the encapsulation of EP and MB in UiO-66-NH_2. In Fig. 2b, the specific absorption peaks of UiO-66-NH_2 are exhibited in the EP@UiO spectra. Not surprisingly, new peaks (1122, 1063, 1019, 989 cm^{-1}) belonging to EP molecule appeared. The results reveal that EP molecules are efficaciously encapsulated in UiO-66-NH_2. Similarly, the encapsulation of MB in UiO-66-NH_2 was effectively verified by the FT-IR spectra in Fig. S4. The DNA functionalization on the surface of UiO-66-NH_2 was characterized by zeta potential (Fig. S5). The loading amounts of MB and EP were characterized through the calibration curve of UV-vis spectrum (Fig. S6).

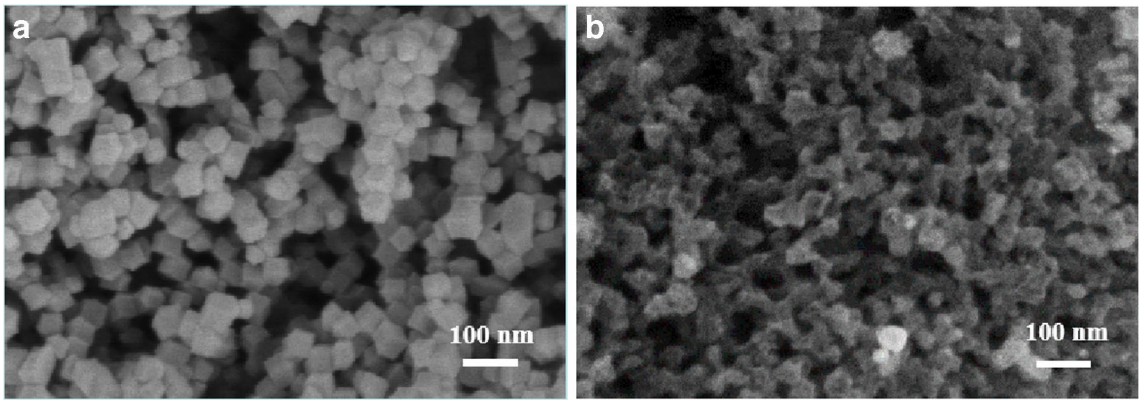

Fig. 1 SEM images of the (**a**) BMZIF and (**b**) NPC

Feasibility of the electrochemical DNA sensor

DPV was employed to verify the electrocatalytic performance of bimetallic ZIF-derived NPC and the electrode modification results. In Fig. 3A, the bare GCE, single ZIF-derived NPC, and bimetallic ZIF-derived NPC were respectively carried out for DPV detection in 0.1 M PB (pH = 7.0) containing EP@UiO, MB@UiO, 10^{-11} M *nuc* gene, and 10^{-11} M *mecA* gene. The DPV peak currents of MB and EP were detected at − 0.14 V and − 0.53 V, respectively. Compared with the peak currents of ZIF-8-derived NPC (curve b) and ZIF-67-derived NPC (curve c), the MB and EP currents have a significant increase at the bimetallic ZIF-derived NPC-modified GCE (curve d). Compared with bare GCE (curve a), the MB and EP currents increase sharply at the bimetallic ZIF-derived NPC-modified GCE. This indicates that the bimetallic ZIF-derived NPC has satisfactory electrocatalytic performance to MB and EP and the electrode is successfully modified.

The feasibility of the EP@UiO and MB@UiO synthesis was characterized by DPV (Fig. S7). Besides, the feasibility of the electrochemical DNA sensor for *nuc* gene and *mecA* gene simultaneous detection was confirmed by DPV (Fig. 3B). When no target exists (curve a), the blank reduction currents of EP and MB are − 0.50 μA and − 0.38 μA. If in the separate presence of 5×10^{-14} M *nuc* gene, the reduction current of EP increases to − 1.85 μA, the current of MB changes slightly. Inversely, when 5×10^{-14} M *mecA* gene exists alone, the reduction current of MB increases to − 1.91 μA. The reduction current of EP shows a slight change. This depends on the target-response electroactive dye release strategy, in which the electroactive dye-encapsulated MOFs are capped by the hybrid dsDNA. When the target exists, it completely hybridizes with displacement DNA (D_{EP}, D_{MB}). So D_{EP} and D_{MB} will be displaced from the MOF surface. In this case, electroactive dyes will be effectively released into the sensing solution. Therefore, two strong current responses are detected when *nuc* gene and *mecA* gene simultaneously exist. The results demonstrate that this homogeneous electrochemical detection strategy can be applied for simultaneous detection of *nuc* and *mecA* gene in MRSA.

Optimization of the assay conditions

To achieve the best experimental results, the following conditions were optimized: (a) the amount of electroactive dyes (EP and MB), (b) the concentration of displacement DNA, (c) the time of hybridization between capture DNA and displacement DNA, and (d) the time of incubation between target DNA and dsDNA-capped UiO-66-NH_2. The results on optimizations are shown in Electronic Supporting Material (S4 and Fig. S8). In brief, the optimal experimental conditions are as follows: (a) the amount of electroactive dyes is 120 μM, (b) the

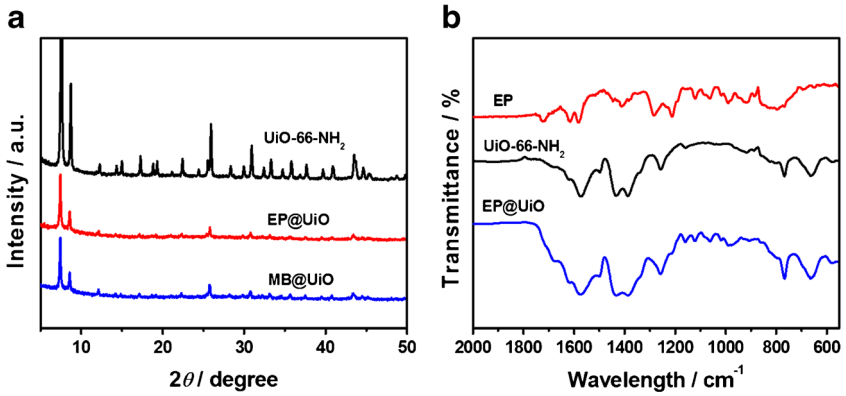

Fig. 2 (**a**) UiO-66-NH_2, EP@UiO, and MB@UiO. (**b**) FT-IR spectra of EP, UiO-66-NH_2, and EP@UiO

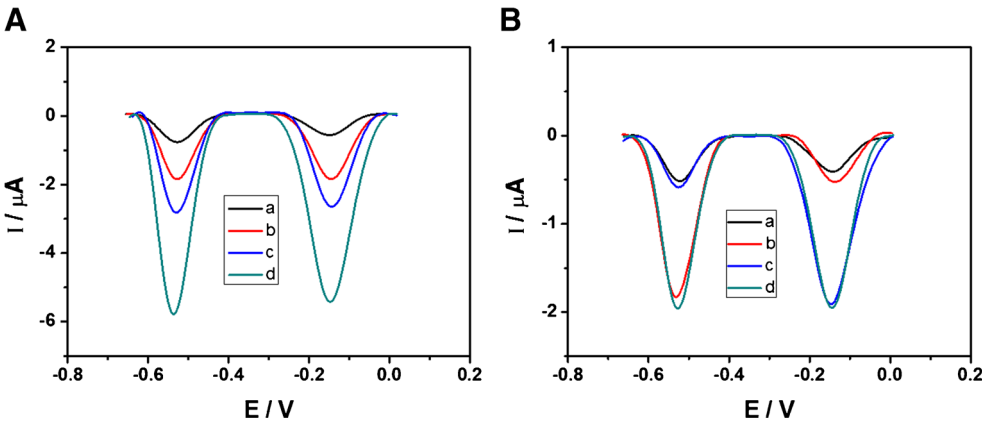

Fig. 3 (A) DPV detection of EP@UiO and MB@UiO under 10^{-11} M *nuc* gene and 10^{-11} M *mecA* gene in 0.1 M PB (pH = 7.0) at the (a) bare GCE, (b) ZIF-8-derived NPC/GCE, (c) ZIF-67-derived NPC/GCE, and (d) bimetallic ZIF-derived NPC/GCE. (B) DPV detection of EP@UiO and MB@UiO under different conditions (a) no target, (b) 5×10^{-14} M *nuc* gene, (c) 5×10^{-14} M *mecA* gene, and (d) 5×10^{-14} M *nuc* gene and 5×10^{-14} M *mecA* gene

concentration of displacement DNA is 700 nM, (c) the time of hybridization between capture DNA and displacement DNA is 60 min, and (d) the time of incubation between target DNA and dsDNA-capped UiO-66-NH_2 is 60 min.

Analytical performance of the DNA biosensor

Based on the optimal assay conditions, the sensitivity of this DNA biosensor was tested by simultaneous detection of *mecA* and *nuc* gene. The change of DPV signal with *mecA* and *nuc* gene concentration is demonstrated in Fig. 4A. When the target DNA concentration synchronously increased from 5×10^{-15} to 5×10^{-10} M, the reduction currents of MB and EP increase with a greater negative value. This is on account of the principle of target-response electroactive dye release, in which more electroactive dyes would be released with the amount of target augments. As shown in Fig. 4B and C, the linear relationship between the DPV signal intensity and the logarithm of DNA concentration is established. The current of EP and MB is linearly dependent on *nuc* gene and *mecA* gene in the range from 5×10^{-15} to 1×10^{-10} M, respectively. For *nuc* gene analysis, the linear equation is $I = -1.38 lgC_{nuc}$-20.4 ($R^2 = 0.996$), and the detection limit (LOD) is 1.6 fM (S/N = 3). For *mecA* gene analysis, the linear equation is $I = -1.31 lgC_{mecA}$-19.1 ($R^2 = 0.998$), and the detection limit (LOD) is 3.7 fM (S/N = 3). Through comparison in Table 1, it can be concluded that the performance of this electrochemical DNA sensor is comparable or advantageous. Importantly, this work makes a progress in simultaneous detection of two different bacterial DNAs. This is attributed to the combination of the stimuli-responsive DNA-gated UiO-66 and NPCs. The UiO-66 is applied as nanocarrier to encapsulate electroactive dyes and release them through target stimuli. The simultaneous detection of other target DNA can be achieved by simply altering the capping DNA. So the stimuli-responsive DNA-gated UiO-66 provides an effective method for multiple target detection. The BMZIF-derived NPCs possess the large surface area and high graphitization degree, which benefits the improvement of electrocatalysis and sensitivity. These properties endow the material a promising application in electrochemical sensor.

Specificity, reproducibility, and stability

Specificity of the electrochemical DNA sensor was verified by analyzing different ssDNA sequences that are related to target DNA. The different ssDNA sequences include one-base mismatched ssDNA (T1), three-base mismatched ssDNA (T2), and non-complementary ssDNA (T3). 1×10^{-11} M target, T1, T2, and T3 were used for DPV detection, respectively. The detection results are shown in Fig. S9. The current change of T3 is extremely small, implying that no hybridization occurs between displacement DNA and T3. After hybridization, the currents of T1 and T2 are much less than that of target, indicating that the target DNA is effectively distinguished from the one-base and three-base mismatched DNA. These results illustrate the prominent specificity of this electrochemical DNA sensor.

The reproducibility of the electrochemical sensor was examined. Five electrodes were fabricated through the same procedure. The 1×10^{-12} M *mecA* gene and *nuc* gene were used for DPV determination. According to the results in Fig. S10A, the relative standard deviation (RSD) of *mecA* gene and *nuc* gene detection is 1.98% and 2.23%, respectively. This indicates the excellent reproducibility of the electrochemical sensor. Stability of the electrochemical sensor was also tested. After storage at 4 °C for 2 weeks, the five uniform electrodes were used to detect 1×10^{-12} M *mecA* gene and *nuc* gene. According to the results in Fig. S10B, 95.6% of the initial current of MB and 95.1% of the initial current of EP are reserved. The results demonstrate the satisfactory stability of this electrochemical sensor.

Detection of MRSA in tap water

This electrochemical DNA sensor was applied to detect target bacteria in tap water. The amplified *mecA* gene band with a

Table 1 Analytical performance of the comparable assays for MRSA DNA detection

Method	Material	Target	Enzyme	DNA labeling	Linearity range/fM	LOD/ fM	Reference
Electrochemistry		*mecA* gene	Yes	Yes	75–2×10^5	63	[26]
Electrochemistry		*mecA* gene	Yes	Yes	10–1×10^7	10	[27]
Fluorescence		*mecA* gene	Yes	No	10–1×10^8	2.4	[28]
Electrochemistry	CS-MWCNTs/AuNPs	*nuc* gene	No	Yes	1–1×10^7	0.33	[29]
Electrochemistry	CS-GR/AuNPs	*nuc* gene	No	Yes	100–1×10^9	33.3	[30]
Electrochemistry	UiO-66/BMZIF-derived NPCs	*mecA* gene/ *nuc* gene	No	No	5–1 × 10^5	1.6/3.7	This work

AuNPs gold nanoparticles, *MWCNTs* multiwalled carbon nanotubes, *CS* chitosan, *GR* graphene, *LOD* limit of detection

size of 127 bp and the amplified *nuc* gene band with a size of 166 bp can be seen in the image of gel electrophoresis (Fig. 5a). As the bacteria concentration decreases from 10^6 to 10^2 CFU mL^{-1}, the concentrations of extracted *mecA* and *nuc* DNA exhibit a decreasing trend. Under low bacteria concentrations, the stripe in gel electrophoresis is hard to observe. As a comparison, the current response of electrochemical DNA sensor changes significantly. The above results demonstrate that this sensor is suitable for MRSA detection in real sample analysis.

Analytical performance towards distinguishing MASA and SA

MRSA and SA can be distinguished because the *mecA* gene is only coded in MRSA. The PCR products of 10^4 CFU mL^{-1}MRSA and SA were detected by DPV. The results are shown in Fig. S11. Two signals of MRSA DNA increase, while the current of *mecA* gene in SA changes slightly. The results indicate that the gene differences are significant for identification of MRSA and SA. Based on the

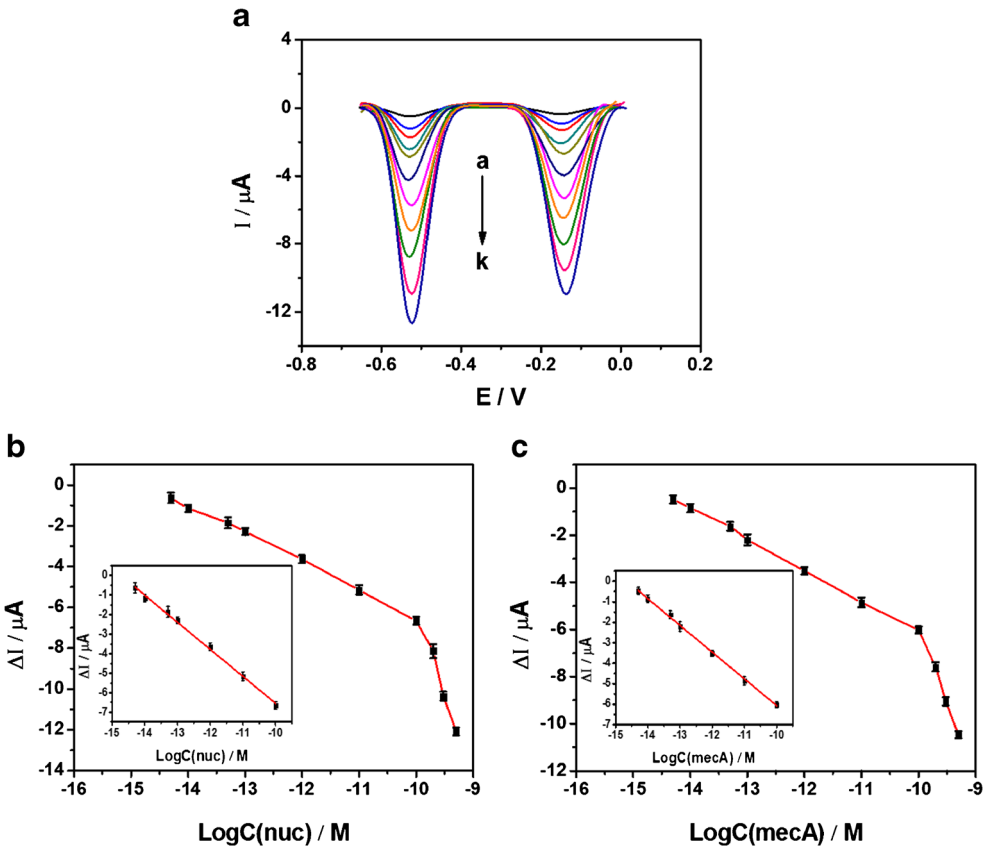

Fig. 4 (A) The DPV response of different concentrations of *nuc* gene and *mecA* gene, (a) 0, 0, (b) 5×10^{-15} M, 5×10^{-15} M, (c) 1×10^{-14} M, 1×10^{-14} M, (d) 5×10^{-14} M, 5×10^{-14} M, (e) 1×10^{-13} M, 1×10^{-13} M, (f) 1×10^{-12} M, 1×10^{-12} M, (g) 1×10^{-11} M, 1×10^{-11} M, (h) 1×10^{-10} M, 1×10^{-10} M, (i) 2×10^{-10} M, 2×10^{-10} M, (j) 3×10^{-10} M, 3×10^{-10} M, (k) 5×10^{-10} M, 5×10^{-10} M. (B) DPV currents change versus *nuc* gene concentrations (lgC_{nuc}). Inset is the linear curve. (C) DPV current changes versus *mecA* gene concentrations (lgC_{mecA}). Inset is the linear curve

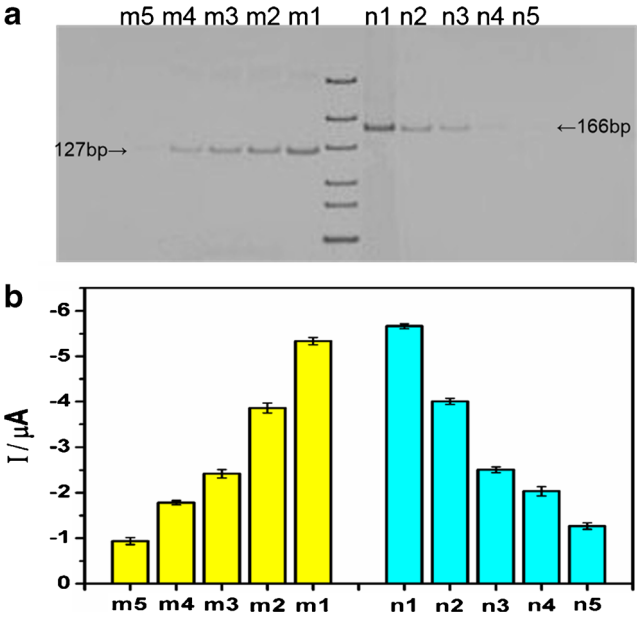

Fig. 5 (**a**) Gel electrophoresis images and (**b**) DPV currents of the PCR amplified *nuc* and *mecA* gene of different MRSA concentrations. m1-m5: PCR amplified *mecA* gene of 10^6–10^2 CFU mL^{-1} MRSA. n1-n5: PCR amplified *nuc* gene of 10^6–10^2 CFU mL^{-1} MRSA

simultaneous detection of the *mecA* gene and *nuc* gene, this sensor can effectively distinguish MRSA and SA.

Analysis MRSA and SA in milk samples

The practical performance of the electrochemical sensor was evaluated by the standard addition methods. Four pretreated milk samples were used for detection. The results are shown in Fig. S12 and Table S2. In sample 2, the DPV current change of MB is extremely small, while the EP current changes a lot. This means that there is SA in the sample 2 but no MRSA. Compared with sample 1, the current change of EP is much greater in samples 3 and 4. This indicates that both MRSA and MA are present in the samples. MRSA is quantitatively detected in each sample, the recovery is between 92.6 and 103%, and the RSD is less than 5%. Meanwhile, SA is successfully identified in each sample. This electrochemical DNA sensor is an effective way for MRSA detection, which has the ability to satisfy practical analysis needs. However, the reproducibility and stability have not reached the level of commercialization. To meet the commercial applications, further improvements, such as the performance of materials and the optimization of strategies, are essentially needed.

Conclusions

A label-free and enzyme-free homogeneous electrochemical DNA sensor was designed for simultaneous detection of *mecA* and *nuc* gene in MRSA. The UiO-66-NH_2 was served as nanocarrier for electroactive dye encapsulation. Based on the target-response electroactive dye release strategy, the electroactive dyes would be released. Co-Zn BMZIF-derived NPCs were applied for electrode modification to improve sensitivity. Combined with these properties, the electrochemical DNA sensor was capable of sensitive detection of *nuc* gene and *mecA* gene. The sensor showed satisfactory performance for MRSA identification in real sample. Besides, MRSA and SA can also be distinguished. More importantly, the electrochemical DNA sensor can be readily designed for simultaneous detection of other target DNA by simply altering the capping DNA. Conclusively, this electrochemical DNA sensor is promising in the biological, medical, and environmental science applications. However, there are still some areas that need further study. It is worth exploring other MOF carriers for more superior sensitivity and stability detection. Besides, in addition to using the DNA-capped MOFs for gene detection, the application of the aptamer-capped MOFs for bacteria detection should be further studied.

Supplementary Information The online version contains supplementary material available at https://doi.org/10.1007/s00604-020-04698-6.

Funding This work was supported by the National Natural Science Foundation of China (grant number 21575042).

Compliance with ethical standards

Conflict of interest There is no conflict of interest in this work.

References

1. Hennekinne J-A, De Buyser M-L, Dragacci S (2012) Staphylococcus aureus and its food poisoning toxins: characterization and outbreak investigation. FEMS Microbiol Rev 36(4):815–836. https://doi.org/10.1111/j.1574-6976.2011.00311.x
2. Ning Y, Zou L, Gao Q, Hu J, Lu F (2018) Graphene oxide-based fluorometric determination of methicillin-resistant Staphylococcus aureus by using target-triggered chain reaction and deoxyribo*nuc*lease-assisted recycling. Microchim Acta 185(3):183. https://doi.org/10.1007/s00604-018-2702-0
3. Zhou G, Wen S, Liu Y, Li R, Zhong X, Feng L, Wang L, Cao B (2011) Development of a DNA microarray for detection and identification of Legionella pneumophila and ten other pathogens in drinking water. Int J Food Microbiol 145(1):293–300. https://doi.org/10.1016/j.ijfoodmicro.2011.01.014
4. Kuroda M, Ohta T, Uchiyama I, Baba T, Yuzawa H, Kobayashi I, Cui LZ, Oguchi A, Aoki K, Nagai Y, Lian JQ, Ito T, Kanamori M, Matsumaru H, Maruyama A, Murakami H, Hosoyama A, Mizutani-Ui Y, Takahashi NK, Sawano T, Inoue R, Kaito C, Sekimizu K, Hirakawa H, Kuhara S, Goto S, Yabuzaki J, Kanehisa M, Yamashita A, Oshima K, Furuya K, Yoshino C, Shiba T, Hattori M, Ogasawara N, Hayashi H, Hiramatsu K (2001) Whole genome sequencing of meticillin-resistant Staphylococcus aureus. Lancet 357(9264):1225–1240. https://doi.org/10.1016/s0140-6736(00)04403-2
5. Yamada K, Jin W, Ohkura T, Murai A, Hayakawa R, Kinoshita K, Mizutani M, Okamoto A, Namikawa T, Ohta M (2013) Detection

of methicillin-resistant Staphylococcus aureus using a specific anti-PBP2a chicken IgY antibody. Jpn J Infect Dis 66(2):103–108. https://doi.org/10.7883/yoken.66.103
6. Nawattanapaiboon K, Kiatpathomchai W, Santanirand P, Vongsakulyanon A, Amarit R, Somboonkaew A, Sutapun B, Srikhirin T (2015) SPR-DNA array for detection of methicillin-resistant Staphylococcus aureus (MRSA) in combination with loop-mediated isothermal amplification. Biosens Bioelectron 74: 335–340. https://doi.org/10.1016/j.bios.2015.06.038
7. Rasheed PA, Sandhyarani N (2017) Electrochemical DNA sensors based on the use of gold nanoparticles: a review on recent developments. Microchim Acta 184(4):981–1000. https://doi.org/10.1007/s00604-017-2143-1
8. Gill AAS, Singh S, Thapliyal N, Karpoormath R (2019) Nanomaterial-based optical and electrochemical techniques for detection of methicillin-resistant Staphylococcus aureus: a review. Microchim Acta 186(2):114. https://doi.org/10.1007/s00604-018-3186-7
9. Costa AM, Kay I, Palladino S (2005) Rapid detection of *mecA* and *nuc* genes in staphylococci by real-time multiplex polymerase chain reaction. Diagn Microbiol Infect Dis 51(1):13–17. https://doi.org/10.1016/j.diagmicrobio.2004.08.014
10. Hulme J (2017) Recent advances in the detection of methicillin resistant Staphylococcus aureus (MRSA). BioChip J 11(2):89–100. https://doi.org/10.1007/s13206-016-1201-9
11. Rubab M, Shahbaz HM, Olaimat AN, Oh D-H (2018) Biosensors for rapid and sensitive detection of Staphylococcus aureus in food. Biosens Bioelectron 105:49–57. https://doi.org/10.1016/j.bios.2018.01.023
12. Ender M, Berger-Baechi B, McCallum N (2009) A novel DNA-binding protein modulating methicillin resistance in Staphylococcus aureus. BMC Microbiol 9:15. https://doi.org/10.1186/1471-2180-9-15
13. Chang J, Wang X, Wang J, Li H, Li F (2019) *Nuc*leic acid-functionalized metal-organic framework-based homogeneous electrochemical biosensor for simultaneous detection of multiple tumor biomarkers. Anal Chem 91(5):3604–3610. https://doi.org/10.1021/acs.analchem.8b05599
14. Sanati A, Jalali M, Raeissi K, Karimzadeh F, Kharaziha M, Mahshid SS, Mahshid S (2019) A review on recent advancements in electrochemical biosensing using carbonaceous nanomaterials. Microchim Acta 186(12):773. https://doi.org/10.1007/s00604-019-3854-2
15. Walcarius A (2018) Silica-based electrochemical sensors and biosensors: recent trends. Curr Opin Electrochem 10:88–97. https://doi.org/10.1016/j.coelec.2018.03.017
16. Anik U, Timur S, Dursun Z (2019) Metal organic frameworks in electrochemical and optical sensing platforms: a review. Microchim Acta 186(3):196. https://doi.org/10.1007/s00604-019-3321-0
17. Cao Y, Wang L, Shen C, Wang C, Hu X, Wang G (2019) An electrochemical sensor on the hierarchically porous Cu-BTC MOF platform for glyphosate determination. Sensors Actuators B Chem 283:487–494. https://doi.org/10.1016/j.snb.2018.12.064
18. Dai G, Li Z, Luo F, Ai S, Chen B, Wang Q (2019) Electrochemical determination of Salmonella typhimurium by using aptamer-loaded gold nanoparticles and a composite prepared from a metal-organic framework (type UiO-67) and graphene. Microchim Acta 186(9): 620. https://doi.org/10.1007/s00604-019-3724-y
19. Kahn JS, Freage L, Enkin N, Garcia MAA, Willner I (2017) Stimuli-responsive DNA-functionalized metal-organic frameworks (MOFs). Adv Mater 29(6). https://doi.org/10.1002/adma.201602782
20. Cao X, Xia J, Meng X, Xu J, Liu Q, Wang Z (2019) Stimuli-responsive DNA-gated nanoscale porous carbon derived from ZIF-8. Adv Funct Mater 29(34):1902237. https://doi.org/10.1002/adfm.201902237
21. Chen W-H, Yu X, Liao W-C, Sohn YS, Cecconello A, Kozell A, Nechushtai R, Willner I (2017) ATP-responsive aptamer-based metal-organic framework nanoparticles (NMOFs) for the controlled release of loads and drugs. Adv Funct Mater 27(37). https://doi.org/10.1002/adfm.201702102
22. Zhang J, Tan Y, Song W-J (2020) Zeolitic imidazolate frameworks for use in electrochemical and optical chemical sensing and biosensing: a review. Microchim Acta 187(4):234. https://doi.org/10.1007/s00604-020-4173-3
23. Wang Z, Yan T, Fang J, Shi L, Zhang D (2016) Nitrogen-doped porous carbon derived from a bimetallic metal-organic framework as highly efficient electrodes for flow-through deionization capacitors. J Mater Chem A 4(28):10858–10868. https://doi.org/10.1039/c6ta02420c
24. Bao T, Fu R, Wen W, Zhang X, Wang S (2020) Target-driven cascade-amplified release of loads from DNA-gated metal-organic frameworks for electrochemical detection of cancer biomarker. ACS Appl Mater Interfaces 12(2):2087–2094. https://doi.org/10.1021/acsami.9b18805
25. Zhang Y, Zhu L, Zhang Y, He P, Wang Q (2018) Simultaneous detection of three foodborne pathogenic bacteria in food samples by microchip capillary electrophoresis in combination with polymerase chain reaction. J Chromatogr A 1555:100–105. https://doi.org/10.1016/j.chroma.2018.04.058
26. Wang T, Zhang Z, Li Y, Xie G (2015) Amplified electrochemical detection of *mecA* gene in methicillin-resistant Staphylococcus aureus based on target recycling amplification and isothermal strand-displacement polymerization reaction. Sensors Actuators B Chem 221:148–154. https://doi.org/10.1016/j.snb.2015.06.057
27. Xu L, Liang W, Wen Y, Wang L, Yang X, Ren S, Jia N, Zuo X, Liu G (2018) An ultrasensitive electrochemical biosensor for the detection of *mecA* gene in methicillin-resistant Staphylococcus aureus. Biosens Bioelectron 99:424–430. https://doi.org/10.1016/j.bios.2017.08.014
28. Li Q, Zhou D, Pan J, Liu Z, Chen J (2018) Ultrasensitive and simple fluorescence biosensor for detection of the *mecA* gene of Staphylococcus aureus by using an exo*nuc*lease III-assisted cascade signal amplification strategy. Analyst 143(23):5670–5675. https://doi.org/10.1039/c8an01805g
29. Sun Y, He X, Ji J, Jia M, Wang Z, Sun X (2015) A highly selective and sensitive electrochemical CS MWCNTs/Au-NPs composite DNA biosensor for Staphylococcus aureus gene sequence detection. Talanta 141:300–306. https://doi.org/10.1016/j.talanta.2015.03.052
30. Niu X, Zheng W, Li X, Zhao W, Wen Z, Li Q, Xie H, Sun W (2018) Electrochemical DNA sensor based on chitosan-graphene and electrodeposited gold nanoparticle modified electrode for the detection of Staphylococcus aureus *nuc* gene sequence. Curr Anal Chem 14(2):159–165. https://doi.org/10.2174/1573411013666170607123122